WSRC-MS-99-00492

The 31st National Symposium on Fatigue and Fracture Mechanics

ASTM Special Technical Publication (STP) No. 1389

Paper ID: 8126

AUTHORS' NAMES:

Y. J. Chao[1], X. K. Zhu[1], P.-S. Lam[2], M. R. Louthan[2], and N. C. Iyer[2]

This document was prepared in conjunction with work accomplished under Contract No. DE-AC09-96SR18500 with the U. S. Department of Energy.

TITLE OF PAPER:

Application of the Two-Parameter J-A_2 Description to Ductile Crack Growth

AUTHORS AFFILIATIONS

1. Department of Mechanical Engineering, University of South Carolina, Columbia,

South Carolina, 29208

2. Savannah River Technology Center, Materials Technology Section,

Westinghouse Savannah River Company, Aiken, South Carolina, 29808

ABSTRACT: Typical ASTM fracture testing determines J-integral resistance (J-R) curve or fracture toughness (J_{IC}) based on specimens with high constraint geometry such as those specified in ASTM E1737-96. A three-term asymptotic solution with two parameters J and A_2 (a constraint parameter) has been developed for characterizing the constraint effect of various geometries. The present paper extends the J-A_2 characterization of a stationary crack tip to the regime of stable crack growth. Similar to the concept of J-controlled crack growth, the J-A_2 description can be approximately used to characterize ductile crack growth under certain amount of crack extension. The region of J-A_2 controlled crack growth is much larger than that controlled by J-integral alone. From the relationships between A_2 and the test dada, J_{IC} and tearing modulus (T_R), the coefficients used to define a J-R curve can be determined. For non-standard specimens or actual structures, once the constraint parameter A_2 is determined, the J-R curves appropriate for these geometries can then be obtained. A procedure of transferring J-R curves determined from the standard ASTM procedure to non-standard specimens or flawed structures is outlined in the paper.

KEYWORDS: constraint effect, fracture toughness, tearing modulus, J-R curve, J-A_2, asymptotic solution, J-controlled crack growth

The ductile failure of engineering materials is characterized by the fracture initiation toughness J_{IC} and the subsequent fracture resistance (J-R) curve. The standard J-R curve shows that J-integral is a function of crack extension and is size-independent within a J-controlled growth region. However, for non-standard, low constraint specimens or flawed structures, the J-R curve may be size and geometry dependent when J-dominance is lost.

The American Society for Testing Materials (ASTM) standardized the specimen geometries for measuring J_{IC} and J-R curves. These specimens are typically high crack-tip constrained, such as the deeply cracked three-point bend (3PB) and the compact tension (CT) specimens which are specified in the ASTM Standard Test Method for J-Integral Characterization of Fracture toughness (E 1737).

Using the ASTM 710 Grade A steel, Hancock et al. [1] measured the fracture toughness J_{IC} and J-R curves for specimens of 3PB, 1CT, center-cracked panel (CCP), and surface cracked panel (SCP). Joyce and Link [2,3] presented the experiment data of ductile crack extension in A533B, HY-100 and HY-80 steels with specimens of 3PB, 1CT, single edge-notched bend (SENB), single edge-notched tensile (SENT), and double edge-cracked plate (DECP). A variety of crack tip constraints were achieved by using these specimens with different crack depths. The results did not show noticeable constraint effects on the crack growth initiation J_{IC}, but a significant difference in the slopes of the J-R curves was observed after some amount of crack growth. Similar results were obtained from ductile crack extension experiments of large-size fracture specimens by Marschall et al. [4], Eisele et al. [5] and Roos et al. [6,7], Kordisch et al. [8], Kelmm et al. [9], Henry et al. [10], and Haynes and Gangloff [11].

Roos et al. [6] showed the dependence of the J-R curve on specimen geometry and specimen thickness for KS01 (22NiMoCr37) which is typically used in German nuclear industry. Their

result indicated that thicker specimen tends to lower the J-R curve. Of particular interest is the J-R curve from the SENT specimen. It is substantially lower than that from the standard CT which is widely used in fracture testing. This implies that the standard ASTM CT specimen may not always form the lower bound J-R curve among various specimen geometries. Therefore, the fracture properties that determined from the standard CT specimens might not safely represent the tearing resistance of an actual structural component. They also showed that in the case of DENT specimens, deeper crack resulted in a lower J-R curve. The trend of all their test data is consistent with a general rule in the constraint effect of fracture, that is, specimens with higher constraint result in lower J-R curves.

In some nuclear applications such as the fracture testing for irradiated materials, the specimen size is limited due to the test facility or the material availability. Miniature or sub-sized disk compact tension (DCT) specimens are often used (Alexander [12]). Similar sub-sized fracture specimens were also used, for instance, by Elliot et al., [13] and Yoon et al. [14], and in ceramics materials used by Zhang and Ardell [15] and Gilbert et al [16]. The J-R curves of this kind of specimens differed significantly from those of standard specimens because of the effect of crack-tip constraints, while the values of initiation toughness J_{IC} remained similar [12].

For a stationary crack in elastic-plastic materials, the effect of constraint on crack-tip fields has been investigated extensively by Betegon and Hancock [17], O'Dowd and Shih [18,19], Yang et al. [20,21] and Chao et al. [22], etc. A review can be found in Chao and Zhu [23]. This paper is focused on the J-A_2 approach [20-22] which was derived from a rigorous asymptotic solution and has been developed for a two-parameter fracture toughness testing. With J being the driving force and A_2 a constraint parameter, this approach has been successfully used to quantify the constraints of crack-tip fields for various geometry and loading configurations [22-

25]. Note that the parameter A_2 is almost independent of its position near the crack tip (Nikishkov et al., [27]).

Similar to the concept of J-controlled crack growth, it is expected that J-A_2 description can approximately characterize the effect of crack-tip constraints on ductile crack growth, at least for certain amount of crack extension. As shown in Figure 1, the amount of J-A_2 controlled crack growth, Δa, should be much larger than that controlled by J alone [23].

The objective of this paper is to extend the J-A_2 characterization of crack tip fields to the stable crack growth regime. A procedure is outlined for transferring the J-R curves determined from ASTM standard specimens to non-standard specimens or to flawed structures. Based on a set of test data, a constraint modified J-R curve can be developed. Using literature data [3], the predicted J-R curve is demonstrated and is compared to the experimental J-R curve.

Theoretical Background

A Mode-I crack under plane strain condition is considered. The elastic-plastic material behavior is described by the Ramberg-Osgood power-law strain hardening curve where the uniaxial strain ε is related to the uniaxial stress σ in simple tension by

$$\frac{\varepsilon}{\varepsilon_0} = \frac{\sigma}{\sigma_0} + \alpha\left(\frac{\sigma}{\sigma_0}\right)^n \qquad (1)$$

where σ_0 is a reference stress, $\varepsilon_0 = \sigma_0 / E$ is a reference strain with E as the Young's modulus, (for actual elastic-plastic solids, σ_0 and ε_0 may be taken as the yield stress and the yield strain of the material, respectively), α is a material constant and n is a strain hardening exponent. By using the J_2 deformation theory of plasticity, the uniaxial stress-strain relation (1) can be generalized to

$$\frac{\varepsilon_{ij}}{\varepsilon_0} = (1+\nu)\frac{\sigma_{ij}}{\sigma_0} - \nu\frac{\sigma_{kk}}{\sigma_0}\delta_{ij} + \frac{3}{2}\alpha\left(\frac{\sigma_e}{\sigma_0}\right)^{n-1}\frac{s_{ij}}{\sigma_0} \quad (2)$$

where ν is the Poisson's ratio, δ_{ij} is the Kronecker delta, s_{ij} is the deviatoric stress and σ_e is the von Mises effective stress defined as $\sigma_e = \sqrt{3s_{ij}s_{ij}/2}$. The tensor summation convention has been used.

J-A_2 three-term asymptotic solution

Equation 2 is rewritten with respect to a polar coordinate system (r, θ) with centered at the crack tip. The $\theta = 0$ is along the uncracked ligament. Yang [28], Yang *et al*. [20,21]) and Chao *et al*. [22] developed a three-term asymptotic crack-tip solution with only two parameters *J* and A_2, in which *J*-integral can be used to quantify the magnitude of applied loading and A_2 describes the crack tip constraints. The asymptotic fields of stress (σ_{ij}), strain (ε_{ij}) and displacement (u_i) can be expressed as

$$\frac{\sigma_{ij}}{\sigma_0} = A_1\left[\left(\frac{r}{L}\right)^{s_1}\tilde{\sigma}_{ij}^{(1)}(\theta,n) + A_2\left(\frac{r}{L}\right)^{s_2}\tilde{\sigma}_{ij}^{(2)}(\theta,n) + A_2^{\,2}\left(\frac{r}{L}\right)^{s_3}\tilde{\sigma}_{ij}^{(3)}(\theta,n)\right] \quad (3)$$

$$\frac{\varepsilon_{ij}}{\alpha\varepsilon_0} = A_1^{\,n}\left[\left(\frac{r}{L}\right)^{ns_1}\tilde{\varepsilon}_{ij}^{(1)}(\theta,n) + A_2\left(\frac{r}{L}\right)^{(n-1)s_1+s_2}\tilde{\varepsilon}_{ij}^{(2)}(\theta,n) + A_2^{\,2}\left(\frac{r}{L}\right)^{(n-1)s_1+s_3}\tilde{\varepsilon}^{*(3)}_{ij}(\theta,n)\right] \quad (4)$$

$$\frac{u_i}{\alpha\varepsilon_0 L} = A_1^{\,n}\left[\left(\frac{r}{L}\right)^{ns_1+1}\tilde{u}_i^{(1)}(\theta,n) + A_2\left(\frac{r}{L}\right)^{(n-1)s_1+s_2+1}\tilde{u}_i^{(2)}(\theta,n) + A_2^{\,2}\left(\frac{r}{L}\right)^{(n-1)s_1+s_3+1}\tilde{u}_i^{(3)}(\theta,n)\right] \quad (5)$$

where the angular functions $\tilde{\sigma}_{ij}^{(k)}$, $\tilde{\varepsilon}_{ij}^{(k)}$ and $\tilde{u}_i^{(k)}$, the stress power exponents s_k, and the dimensionless integration constant I_n are only dependent of the hardening exponent n and independent of the other material constants (i.e. α, ε_0, σ_0) and applied load. The characteristic length, L, can be the crack length a, the specimen width W, the thickness B or an unity 1 cm. The parameters A_1 and s_1 are given by the Hutchinson-Rice-Rosengren (HRR) field [29-31],

$$A_1 = \left(\frac{J}{\alpha \varepsilon_0 \sigma_0 I_n L} \right)^{-s_1}, \qquad s_1 = -\frac{1}{n+1} \tag{6}$$

and $s_3 = 2s_2 - s_1$ for $n \geq 3$. The parameter A_2 is undetermined and is related to the loading and geometry of specimen. Plane strain Mode I dimensionless functions $\tilde{\sigma}_{ij}^{(k)}$, $\tilde{\varepsilon}_{ij}^{(k)}$, $\tilde{u}_i^{(k)}$, s_k and I_n have been calculated and tabulated by Chao and Zhang [32]. When $A_2 = 0$, the three-term asymptotic solutions (3) - (5) coincide with the HRR singular field.

Yang et al. [20] showed that the above three-term asymptotic solutions are the fully plastic or the pure power-law solutions when the material is moderate or low strain hardening, $n \geq 3$. Comparing with the finite element results, it can be shown that the three-term solution can be used to characterize the crack tip region well beyond $r / (J / \sigma_0) = 5$ [20,21,23,26]. This solution is valid under both small scale yielding and large scale yielding conditions, and is independent of the crack tip constraint in any strain hardening materials.

Relationship between J and A_2 under fully plastic conditions

For a pure power-law or fully plastic material, Ilyushin [33] showed that under monotonically increasing load a solution to the boundary value problem has a simple form, that

is, the stress is linearly related to the applied load P, the strain and the displacement are proportional to P^{n}. Therefore,

$$\frac{\sigma_{ij}}{\sigma_0} = \left[\frac{P}{P_0}\right]\hat{\sigma}_{ij}(x_i, n) \tag{7}$$

$$\frac{\varepsilon_{ij}}{\alpha\varepsilon_0} = \left[\frac{P}{P_0}\right]^{n}\hat{\varepsilon}_{ij}(x_i, n) \tag{8}$$

$$\frac{u_j}{\alpha\varepsilon_0 L} = \left[\frac{P}{P_0}\right]^{n}\hat{u}_i(x_i, n) \tag{9}$$

where the dimensionless $\hat{\sigma}_{ij}$, $\hat{\varepsilon}_{ij}$ and $\hat{u}_i$ are functions of spatial coordinates x_i and strain hardening exponent n, and are independent of the applied load P. The reference load, P_0, can be the limit load. These expressions are the direct result of the homogenous nature of the equations of equilibrium, compatibility, and the constitutive relation (2).

Since the integrand of the J-integral involves products of stress and displacement gradients, from (7) - (9), Goldman and Hutchinson [34] showed that the fully plastic J-integral is proportional to P^{n+1}:

$$\frac{J}{\alpha\varepsilon_0\sigma_0 a} = \left[\frac{P}{P_0}\right]^{n+1}\hat{J}(a/W, n) \tag{10}$$

where a is a crack length, W is a specimen width. The dimensionless function $\hat{J}$ depends only on the geometry size ratio a/W and strain hardening exponent n.

Substituting (10) into (7) - (9) and eliminating load term P/P_0, one can obtain the relationship between the field quantities and J-integral

$$\frac{\sigma_{ij}}{\sigma_0} = \left[\frac{J}{\alpha\varepsilon_0\sigma_0 a\hat{J}(a/W,n)}\right]^{\frac{1}{n+1}} \hat{\sigma}_{ij}(x_i,n) \tag{11}$$

$$\frac{\varepsilon_{ij}}{\alpha\varepsilon_0} = \left[\frac{J}{\alpha\varepsilon_0\sigma_0 a\hat{J}(a/W,n)}\right]^{\frac{n}{n+1}} \hat{\varepsilon}_{ij}(x_i,n) \tag{12}$$

$$\frac{u_j}{\alpha\varepsilon_0 L} = \left[\frac{J}{\alpha\varepsilon_0\sigma_0 a\hat{J}(a/W,n)}\right]^{\frac{n}{n+1}} \hat{u}_i(x_i,n) \tag{13}$$

The above expressions are the unique forms of solutions for plane crack problems under fully plastic deformation. Therefore, the three-term asymptotic solutions (3) - (5) must meet the functional forms (11) - (13), or

$$\left(\frac{r}{L}\right)^{s_1}\tilde{\sigma}_{ij}^{(1)}(\theta) + A_2\left(\frac{r}{L}\right)^{s_2}\tilde{\sigma}_{ij}^{(2)}(\theta) + A_2^{\,2}\left(\frac{r}{L}\right)^{s_3}\tilde{\sigma}_{ij}^{(3)}(\theta) = \left[\frac{I_n L}{a\hat{J}(a/W,n)}\right]^{\frac{1}{n+1}}\hat{\sigma}_{ij}(r,\theta,n) \tag{14}$$

$$\left(\frac{r}{L}\right)^{ns_1}\tilde{\varepsilon}_{ij}^{(1)}(\theta) + A_2\left(\frac{r}{L}\right)^{(n-1)s_1+s_2}\tilde{\varepsilon}_{ij}^{(2)}(\theta) + A_2^{\,2}\left(\frac{r}{L}\right)^{(n-1)s_1+s_3}\tilde{\varepsilon}^{*(3)}_{ij}(\theta) = \left[\frac{I_n L}{a\hat{J}(a/W,n)}\right]^{\frac{n}{n+1}}\hat{\varepsilon}_{ij}(r,\theta,n) \tag{15}$$

$$\left(\frac{r}{L}\right)^{ns_1+1}\tilde{u}_i^{(1)}(\theta) + A_2\left(\frac{r}{L}\right)^{(n-1)s_1+s_2+1}\tilde{u}_i^{(2)}(\theta) + A_2^{\,2}\left(\frac{r}{L}\right)^{(n-1)s_1+s_3+1}\tilde{u}_i^{(3)}(\theta) = \left[\frac{I_n L}{a\hat{J}(a/W,n)}\right]^{\frac{n}{n+1}}\hat{u}_i(r,\theta,n) \tag{16}$$

In equations (14) - (16), the exponents s_k and the constant I_n are only dependent of the hardening exponent n. The angular functions $\tilde{\sigma}_{ij}^{(k)}(\theta)$, $\tilde{\varepsilon}_{ij}^{(k)}(\theta)$ and $\tilde{u}_i^{(k)}(\theta)$, the dimensionless quantities $\hat{\sigma}_{ij}$, $\hat{\varepsilon}_{ij}$ and $\hat{u}_i$ are the functions of polar coordinates (r, q) and hardening exponent n. The

dimensionless function $\hat{J}$ depends upon geometry size ratio *a/W* and hardening exponent *n*. Moreover, all these quantities are independent of the other material properties (α, ε_0, σ_0) and the level of the applied load or *J*-integral. If the characteristic length *L* is independent of *J*, for instance, *L* = *a*, *W*, *B* or 1 cm, one can conclude immediately from (14)-(16) that A_2 is only the function of strain hardening exponent *n* and geometry dimension (*a*, *W*, *a/W*), namely,

$$A_2\big|_{\text{fully plastic}} = f(n,\ \textit{geometry}) \tag{17}$$

As a result, under fully plastic deformation conditions the constraint parameter A_2 in the three-term solutions (3) - (5) are independent of the applied J for a given specimen and material.

Using a 3PB and SEN specimens, the finite element results [22,28] showed that A_2 becomes a constant value as the applied load (characterized by J) increases beyond about 1.2 times limit load with the hardening exponent $n = 4$, 7 and 12. Therefore, for a specimen fracturing at large-scale yielding or near fully plastic condition, the value of A_2 determined at $J = J_{IC}$ can be used for loads $J \geq J_{IC}$, as long as the growing crack tip is still within the *J*-A_2 field and the elastic unloading behind the crack tip does not significantly alter the crack tip field.

Determination of the constraint parameter A_2

A *point matching technique* was used by Yang et al. [20,21] and Chao et al. [22] to determined the value of A_2. The stress obtained by finite element analysis at a point (r, θ) near the crack tip is set equal to the three-term analytical solution (3) to solve for A_2. In particular, these authors used σ_{rr} and $\sigma_{\theta\theta}$ at $r = 2(J/\sigma_0)$, $\theta = 0^\circ$ or 45°. Chao and Zhu [23] also used this approach to determine A_2, but r is chosen from J/σ_0 to $5(J/\sigma_0)$.

To reduce the finite element mesh size sensitivity on the value of A_2, Nikishkov *et al*. [27] developed another technique, the *least square procedure,* for fitting the finite element data in the region $1 < r/(J/\sigma_0) < 5$. They found that A_2 is almost independent of its location within the region of interest.

A *simple weight average technique* is developed for the determination of A_2. It is assumed that the resultant force due to the crack opening stress $\sigma_{\theta\theta}(r,0)$ on the remaining ligament in the region of $1 < r/(J/s_0) < 5$ has the same magnitude from a finite element result and from the three-term solution (3). Mathematically it is expressed as

$$\int_1^5 \frac{\sigma_{\theta\theta}^{FEA}(\bar{r},0)}{\sigma_0} d\bar{r} = \left(\frac{J}{\alpha\varepsilon_0\sigma_0 I_n L}\right)^{-s_1} \int_1^5 \left[\left(\frac{J\bar{r}}{\sigma_0 L}\right)^{s_1} \tilde{\sigma}_{ij}^{(1)}(0) + A_2\left(\frac{J\bar{r}}{\sigma_0 L}\right)^{s_2} \tilde{\sigma}_{ij}^{(2)}(0) + A_2^{\,2}\left(\frac{J\bar{r}}{\sigma_0 L}\right)^{s_3} \tilde{\sigma}_{ij}^{(3)}(0)\right] d\bar{r}$$

where $\bar{r} = r/(J/\sigma_0)$ and $\sigma_{\theta\theta}^{FEA}$ is the crack opening stress for points on the (r,θ) = (r, 0) line determined from finite element calculations. Upon integrating the above expression, the value of A_2 can be determined simply by solving the following second-order algebraic equation:

$$aA_2^{\,2} + bA_2 + c = 0 \tag{18}$$

where

$$a = \frac{5^{s_3+1} - 1}{(s_3+1)(L\sigma_0/J)^{s_3}} \tilde{\sigma}_{\theta\theta}^{(3)}(0) \tag{19a}$$

$$b = \frac{5^{s_2+1} - 1}{(s_2+1)(L\sigma_0/J)^{s_2}} \tilde{\sigma}_{\theta\theta}^{(2)}(0) \tag{19b}$$

$$c = \frac{5^{s_1+1} - 1}{(s_1+1)(L\sigma_0/J)^{s_1}} \tilde{\sigma}_{\theta\theta}^{(1)}(0) - \left(\frac{J}{\alpha\varepsilon_0\sigma_0 I_n L}\right)^{s_1} \int_1^5 \frac{\sigma_{\theta\theta}^{FEA}(\bar{r},0)}{\sigma_0} d\bar{r} \tag{19c}$$

The integration in (19c) can be determined approximately by numerical summation of $\sigma_{\theta\theta}^{FEA}(\bar{r},0)$ on the finite element nodes in $1<\bar{r}<5$. Note that the weight averaging in (18) and (19) determines the averaged value for A_2 within the range $1<\bar{r}<5$ along the (r, 0) line. Other ranges of $\bar{r}$ for averaging A_2 may be used.

J-A_2 description of ductile crack growth

The two-parameter, J-A_2 three-term solution has been successfully used to quantify the effect of constraint for stationary crack-tip fields with various geometries and loading configurations [20-22,26]. For a growing crack, similar to the concept of *J*-controlled crack growth, it is assumed that that, within certain amount of crack extension, the *J*-A_2 description can approximately characterize the effect of geometry constraint on ductile crack growth with *J* being the driving force and A_2 the constraint parameter. It is expected that the amount of *J*-A_2 controlled crack growth is much larger than that of the *J*-controlled since the crack tip zone dominated by the *J*-A_2 is much larger than that controlled by *J* alone [23].

A procedure for transferring the *J*-*R* curve determined from a standard ASTM procedure to that for a non-standard specimen or to a flawed structure is described in the following. It is then illustrated by using the test data (J_{IC} and T_R) of Joyce and Link [3]. A constraint based *J*-*R* curve is established for the case of stable crack growth which is characterized by the parameter A_2.

General framework to construct constraint-modified J-R curves

The ASTM E 1737 specifies test procedures for the determination of fracture toughness as characterized by the *J*-Integral under plane strain conditions. Based on the amount of crack extension, three toughness properties are identified as: (*a*) instability without significant prior crack extension (J_C); (*b*) onset of stable crack extension (J_{IC}); (*c*) stable crack growth resistance curve (*J*-*R*) in the region of *J*-controlled growth. The present investigation is focused on the last two fracture properties, (*b*) and (*c*).

It is specified in ASTM E 1737 that the fracture toughness J_{IC} is defined as the value of *J* at crack extension $\Delta a = \Delta a_Q = \frac{J_{IC}}{2s_F} + 0.2\,(\text{mm})$ or

$$J_{IC}(\Delta a) = J(\Delta a_Q)\Big|_{\Delta a_Q = \frac{J_{IC}}{2s_F} + 0.2\,(\text{mm})} \tag{20}$$

where σ_F is the flow stress or effective yield stress. In addition, the *J*-resistance curve can be approximated by a best-fit power-law relationship,

$$J(\Delta a) = C_1 \left(\frac{\Delta a}{k} \right)^{C_2} \tag{21}$$

where the coefficients C_1 and C_2 are constants, and $k = 1\,\text{mm}$ or $1\,\text{inch}$ depending on the unit of Δa. Note that equation (21) assumes $J = 0$ at $\Delta a = 0$.

Since J_{IC} corresponds to crack initiation, the constraint parameter A_2 can be solved from equation (18) by matching the three-term solution (3) to the finite element results at load level J_{IC}. If the specimens are nonstandard, the corresponding value of A_2 can be obtained in a similar manner, as long as the J_{IC} value is measured.

As described earlier, under large scale yielding or near fully plastic deformation, the constraint parameter A_2 determined at $J = J_{IC}$ remains a constant for $J \geq J_{IC}$ in the case of a stationary crack. If the crack extension incurs and the location of the current crack tip is within the *J*-A_2 dominant region, the value of A_2 is approximately invariant for the specific specimen. Incorporating the constraint effect into the *J*-*R* curve, a curve of *J* versus crack extension Δa under *J*-A_2 controlled growth can be expressed as

$$J(\Delta a, A_2) = C_0(A_2) + C_1(A_2)\left(\frac{\Delta a}{k}\right)^{C_2(A_2)} \tag{22}$$

The coefficients $C_0(A_2)$, $C_1(A_2)$, $C_2(A_2)$ are unknown constants and depend upon the constraint A_2 at the crack tip for a specific material and specimen. The coefficient $C_0(A_2)$ is added to include the fact that *J* is nonzero at zero crack extension (Δa). That is, if the J value is known prior to crack initiation, then

$$C_0(A_2) = J(\Delta a = 0, A_2) \equiv J_0(A_2) \tag{23}$$

Equation (22) extends the current ASTM *J*-resistance curve concept of $J(\Delta a)$ to a constraint modified *J*-resistance curve $J(\Delta a, A_2)$. Once the functional forms of $C_0(A_2)$, $C_1(A_2)$ and $C_2(A_2)$ are known, the constraint modified *J*-resistance curve (or function), (22), is completely determined. The determination of $C_0(A_2)$, $C_1(A_2)$ and $C_2(A_2)$ is described in the following steps:

Step 1: J-R curves are determined experimentally based on ASTM procedures, but for different crack sizes or specimen types, as shown in Figure 2(a). The test specimens should be chosen to include several low constraint to high constraint specimens. As shown in Figure 2(a), each *J*-*R*

curve has a constant A_2 value, which is determined at the crack initiation load using finite element results and equation (18).

Step 2: Using three points on each *J-R* curve as shown in Figure 2(a) the three coefficients $C_0(A_2)$, $C_1(A_2)$ and $C_2(A_2)$ can be determined for each *J-R* curve or A_2. That is

$$C_1(A_2)\left(\frac{\ddot{A}\Delta a_i}{k}\right)^{C_2(A_2)} = J_i(\Delta a_i, A_2) - C_0(A_2); \qquad \text{i} = 1, 2, 3 \tag{24}$$

If $\Delta a = \Delta a_Q = \frac{J_{IC}}{2\sigma_F} + 0.2\,(\text{mm})$, $k = 1mm$ and the International System of Units (SI) units are used, one has

$$C_1(A_2)\left(\frac{J_{IC}}{2k\sigma_F} + 0.2\right)^{C_2(A_2)} = J_{IC}(A_2) - C_0(A_2) \tag{25}$$

Step 3: The step 2 is repeated for several *J-R* curves, see Figure 2(a). Through curve fitting, the functional forms of $C_0(A_2)$, $C_1(A_2)$ and $C_2(A_2)$ are determined as shown in Figure 2(b).

Alternatively, these coefficients can be determined by the values of the initiation fracture toughness J_{IC} and the corresponding tearing modulus T_R. Note that the current ASTM E 1737 specifies detailed procedures for the determination of J_{IC} (J at $\Delta a = \Delta a_Q = \frac{J_{IC}}{2\sigma_F} + 0.2\,mm$) and $T_R = \frac{E}{\sigma_0^2}\frac{dJ}{da}$ at $\Delta a = 1$ mm. The fracture toughness at $\Delta a = 0$ is often close to zero, as assumed in (21). The constraint modified *J-R* curve, equation (22), has therefore only two coefficients $C_1(A_2)$ and $C_2(A_2)$ for each curve or A_2, which can then be determined by J_{IC} and T_R. Using

(22) and (25) with SI units, one obtains the following two equations to determine the unknown coefficients C_1 and C_2:

$$C_1(A_2)\left(\frac{J_{IC}}{2k\sigma_F}+0.2\right)^{C_2(A_2)} = J_{IC}(A_2)$$
$$C_1(A_2)C_2(A_2) = \left.\frac{\partial J(\Delta a, A_2)}{\partial a}\right|_{\Delta a=1mm} = T_R(A_2)\frac{\sigma_0^2}{E} \qquad (26)$$

Note that both the initiation fracture toughness J_{IC} and the tearing modulus $T_R = \frac{E}{\sigma_0^2}\frac{dJ}{da}$ are now functions of the constraint parameter A_2. Using the J-R curves obtained for several specimens of various constraint levels, the functional relationship on the right hand sides of (26) can be established as shown in Figures 3(a) and 3(b). For a given A_2 value (e.g. A_2 from 0 to –1.0), solving equation (26) gives the solutions for C_1 and C_2. Consequently, the functional forms of $C_1(A_2)$ and $C_2(A_2)$ are obtained by curve fitting as shown in Figure 3(c).

Once the constraint modified *J-R* curve, equation (22), is completely determined for a material of interest, the *J-R* curves appropriate for any test specimen or for any structural component can then be obtained, provided that the value of the constraint parameter A_2 is known.

Experimental results of Joyce and Link (1997)

Following ASTM E 1737, Joyce and Link [3] tested a series of SENB specimens with *a/W* ratios ranging from 0.13 to 0.83 for the HY80 steel. The material properties[1] are: 0.2% yield

[1] Joyce, J. A., Private communication, 1998.

strength $\sigma_0 = 610\,MPa$, ultimate strength $\sigma_{us} = 726\,MPa$, Young's modulus E = 199 *GPa*, Poisson ratio $\nu = 0.29$, and the strain hardening exponent $n = 10$.

The initiation fracture toughness J_{IC} and the material tearing resistance T_R at $\Delta a = 1\text{mm}$, obtained with ASTM E 1737 are presented by Joyce and Link [3] for all specimens and reproduced in Table 1. Because there is a simple relation between the Q-stress [18] and the A_2 parameter, the A_2 parameter in the current analysis was obtained by converting the Q-stress reported by Joyce and Link [3].

Comparing (3) to the definition of Q, that is, $Q\sigma_0 = \sigma_{\theta\theta} - \sigma_{\theta\theta}^{HRR}$ at $\theta = 0$ and $r = 2J/\sigma_0$, the relationship between Q and A_2 is

$$A_2\left(\frac{2J}{\sigma_0 L}\right)^{s_2}\tilde{\sigma}_{\theta\theta}^{(2)}(0) + A_2^{\,2}\left(\frac{2J}{\sigma_0 L}\right)^{s_2}\tilde{\sigma}_{\theta\theta}^{(2)}(0) = Q\left(\frac{J}{\alpha\varepsilon_0\sigma_0 I_n L}\right)^{s_1} \tag{27a}$$

For strain hardening exponent $n = 10$, the following constants were determined: $s_1 = -0.09091$, $s_2 = 0.06977$, $s_3 = 0.23044$, $I_n = 4.53985$, $\tilde{\sigma}_{\theta\theta}^{(2)} = 0.3130$, and $\tilde{\sigma}_{\theta\theta}^{(3)}(0) = -6.4127$. Letting $\alpha = 1$ and $L = 10\,mm$, (27a) becomes

$$0.313\left(\frac{J}{3050}\right)^{0.06977} A_2 - 6.4127\left(\frac{J}{3050}\right)^{0.23044} A_2^2 = \left(\frac{84.882}{J}\right)^{0.09091} Q \tag{27b}$$

Using (27b) and the Q-stresses which were reported by Joyce and Link [3], the A_2 values were determined and are listed in Table 1.

Prediction of J-R curves using the J-A_2 description

With the data given in Table 1 and following the procedures described earlier, a constraint-modified *J-R* curve can be constructed. Figures 4(a) and 4(b) show plots of J_{IC} and T_R versus A_2, respectively. Note that the relationship of J_{IC} and A_2 can be fitted linearly by

$$J_{IC} = - 119.79\, A_2 + 161.86 \quad (\text{kJ/m}^2) \tag{28}$$

From Figure 4(a), it can be seen that J_{IC} may be approximated by

$$J_{IC} = 194 \quad (\text{kJ/m}^2) \tag{29}$$

In Figure 4(b), the relationship of T_R and A_2 is fitted by a straight line

$$T_R = - 187.33\, A_2 + 36.425 \tag{30}$$

or by a quadratic equation

$$T_R = -164.77\, A_2^2 - 277.38\, A_2 + 25.717 \tag{31}$$

Figure 4(b) shows that (30) and (31) are almost indistinguishable. Therefore, the linear equation (30) is used in this analysis.

Based on (30) and the definition of material tearing resistance $T_R = \dfrac{E}{\sigma_0^2}\dfrac{\partial J}{\partial a}\Big|_{\Delta a = 1mm}$, substitution of material properties (E and s_0) yields the slope of the J-R curve at $\Delta a = 1\,mm$:

$$\left.\frac{\partial J}{\partial a}\right|_{\Delta a = 1mm} = -350.31 A_2 + 68.109 \qquad (\text{N/mm}^2) \tag{32}$$

J-R curves with J_{IC} independent of constraint – The material flow stress of HY80 is 668 MPa and is defined as $\sigma_F = \dfrac{1}{2}(\sigma_0 + \sigma_{us})$. Substituting (29) and (32) into (26) gives

$$\begin{cases} C_1 (0.3452)^{C_2} = 194 \\ C_1 C_2 = -350.31 A_2 + 68.109 \end{cases} \tag{33}$$

For a specific value of A_2, the coefficients C_1 and C_2 can be solved from (33) with a non-linear Newton iteration method. Within the range $-1.0 \le A_2 \le 0$, the values of C_1 and C_2 are plotted in Figures 5(a) and 5(b), respectively. They are expressed as

$$\begin{aligned} C_1(A_2) &= -226.35A_2 + 264.63 \\ C_2(A_2) &= -0.5813A_2 + 0.3182 \end{aligned} \tag{34}$$

By substituting (34) into (22), the constraint modified *J-R* curve for HY-80 steel is found to be

$$J(\Delta a,\ A_2) = (-226.35A_2 + 264.63)\left(\frac{\Delta a}{1mm}\right)^{(-0.5813A_2 + 0.3182)} \tag{35}$$

J-R curves with J_{IC} linearly related to constraint A_2 - It is not uncommon that the fracture toughness J_{IC} is weakly dependent of the specimen geometry. Therefore, equation (28) is used to investigate the effect of J_{IC} - A_2 relationship on the *J-R* curves. Following the same procedure and by substituting (28) and (32) into (26), it can be shown that

$$\begin{cases} C_1(0.3212 - 0.0897A_2)^{C_2} = -119.79A_2 + 161.86 \\ C_1C_2 = -350.31A_2 + 68.109 \end{cases} \tag{36}$$

Solving (36) for a given value of A_2, the coefficients C_1 and C_2 are obtained and are plotted in Figures 6(a) and 6(b), respectively. For $-1.0 \le A_2 \le 0$, the expressions for C_1 and C_2 are, respectively,

$$\begin{aligned} C_1(A_2) &= -323.15A_2 + 237.78 \\ C_2(A_2) &= -0.4365A_2 + 0.3551 \end{aligned} \tag{37}$$

Substituting (37) into (22), the constraint modified *J-R* curve for HY-80 steel is obtained:

$$J(\Delta a,\ A_2) = (-323.15A_2 + 237.78)\left(\frac{\Delta a}{1mm}\right)^{(-0.4365A_2 + 0.3551)} \qquad (38)$$

Figure 7 shows the *J-R* curves predicted by (35), solid curves, and by (38), dashed curves, for several A_2 values (0.0, -0.168, -0.2, -0.3, and -0.4). It indicates that the predicted *J-R* curves are insensitive to the functional forms of J_{IC}. Therefore, J_{IC} can be approximately considered as a material constant and is independent of the level of constraint. This agrees with the experimental observations of Hancock et al.[1] and Joyce and Link [3].

Some experimental data of Joyce and Link [3] are also included in Figure 7. The predicted J-R curves (A_2= -0.168 and -0.393) are compared with the test data of a shallow crack specimen (a/W=0.13) and a deep crack specimen (a/W=0.55). Note that the present analysis used only two data points from each of the specimen of Joyce and Link, namely, J_{IC} at $\Delta a \cong 0.35mm$ and T_R at $\Delta a = 1$ mm , and yet the predicted J-R curves match very well with the experimental data up to $\Delta a = 7mm$. Therefore, the *J-A*$_2$ description can successfully predict the *J*-resistance curves even considerable amount of crack growth has occurred.

Conclusions

To quantity the crack tip constraint effect on *J-R* curves in ductile crack growth, this paper extends the concept of *J*-controlled crack growth to *J-A*$_2$ controlled crack growth, in which the J-integral represents the load level and the A_2 parameter indicates the level of constraint. The main results are summarized as follows:

(1) Under a fully plastic condition, it is proved by the deformation theory of plasticity (Ilyushin [33]) that the constraint parameter A_2 is independent of the applied load. As a result,

the constraint parameter A_2, determined at the crack initiation (J_{IC}), remains invariant as long as the growing crack tip is still within a J-A_2 controlled regime.

(2) A simple weight average technique is developed to evaluate the value of A_2 by matching the finite element result with the three-term asymptotic solution [20-22]. The value of A_2 determined in this manner is almost independent of the distance from the crack tip within $1 \le r/(J/\sigma_0) \le 5$, where the fracture event normally takes place.

(3) Using A_2 as a constraint parameter, the concept of a constraint modified *J-R* curve is proposed. A procedure is outlined for transferring the *J-R* curves determined from the ASTM standards to non-standard specimens or to structures with flaws. Once the constraint parameter A_2 is determined, the *J-R* curve for any specimen can be readily predicted.

(4) The methodology of the constraint modified *J-R* curve has been applied to a set of SENB test data obtained by Joyce and Link [3]. Using the initiation fracture toughness J_{IC} and the tearing modulus T_R, the constraint modified *J-R* curves are constructed for the test material. The predicted J-R curves agree very well with the experimental data up to a crack extension of 7 mm. Note that only two test data points (J_{IC} and T_R measured at $\Delta a < 1\,\text{mm}$) were needed to successfully construct the constraint modified J-R curve. These results also indicate that (a) a nearly linear relationship exists between the slope of the material *J*-resistance curve at 1 mm of crack extension and the constraint parameter A_2; and (b) the predicted *J-R* curves are insensitive to the value of J_{IC} which may be weakly dependent of the crack tip constraint. Therefore, it can be concluded that the initiation fracture toughness J_{IC} may be regarded as a constant and is independent of the crack tip constraint. This was proposed earlier by Hancock et al. [1] and Joyce and Link [3].

References

[1] Hancock, J. W., Reuter, W. G. and Parks, D. M., Constraint and toughness parameterized by *T*, *Constraint effects in fracture, ASTM STP 1171*, American society of Testing and Materials, Philadelphia, 1993, pp.21-40.

[2] Joyce, J. A. and Link, R. E., Effects of constraint on upper shelf fracture toughness, *Fracture Mechanics: 26th Volume, ASTM STP 1256*, American Society for Testing and Materials, Philadelphia, 1995, pp.142-177.

[3] Joyce, J. A. and Link, R. E., Application of two parameter elastic-plastic fracture mechanics to analysis of structures, *Engineering Fracture Mechanics*, Vol.57, 1997, pp.431-446.

[4] Marschall, C. W., Papaspyropoulos, V. and Landow, M. P., Evaluation of attempts to predict large-crack-growth *J-R* curves from small specimen tests, *Nonlinear Fracture Mechanics*: *Volume II – Elastic Plastic Fracture, ASTM STP 995*, American Society of Testing and Materials, Philadelphia, 1989, pp.123-143.

[5] Eisele, U., Roos, E., Seidenfuss, M. and Silcher, Determination of *J*-integral-based crack resistance curve and initiation values for the assessment of cracked large-scale specimens, *Fracture Mechanics: twenty-second symposium (Volume I), ASTM STP 1133*, American Society for Testing and Materials, Philadelphia, 1992, pp.37-59.

[6] Roos, E., Eisele, U. and Silcher, H., Effect of stress state on the ductile fracture behavior of large scale specimens, *Constraint effects in fracture, ASTM STP 1171*, American Society for Testing and Materials, Philadelphia, 1993, pp.41-63.

[7] Roos, E., Eisels, U., Silcher, H. and Eckert, W., Impact of the stress state on the fracture mechanics of heavy section steel component failure mechanics, *Fracture Mechanics*

Verification by Large-Scale Testing, EGF/ESIS8 (Edited by K. Kussmaul), 1991, pp.65-85.

[8] Kordisch, H., Sommer, E. and Schmitt, W., The influence of triaxiality on stable crack growth, *Nuclear Engineering and Design*, Vol.112, 1989, pp.27-35.

[9] Klemm, W., Memhard, D. and Schmitt, W., Experimental and numerical investigation of surface cracks in plates and pipes, *Fracture Mechanics Verification by Large-Scale Testing*, EGF/ESIS8 (Edited by K. Kussmaul), 1991, pp.139-150.

[10] Henry, B. S., Luxmoore, A. R. and Sumpter, J. D. G., Elastic-plastic fracture mechanics assessment of low constraint aluminium test specimens, *International Journal of Fracture*, Vol.81, 1996, pp.217-234.

[11] Haynes, M. J. and Gangloff, R. P., High resolution *R*-curve characterization of the fracture toughness of thin sheet aluminum alloys, *Journal of Testing and Evaluation*, Vol. 25, 1997, pp.82-98.

[12] Alexander, D. J., Fracture toughness measurements with subsize Disk Compact specimens, *Small Specimens Test Techniques Applied to Nuclear Reactor Vessel Thermal Annealing and Plant Life Extension, ASTM STP 1204*, American Society of Testing and Materials, Philadelphia, 1993, pp.130-142.

[13] Elliot, C., Emark, M., Lucas, G. E., et al., Development of disk compact tension specimens and test techniques for HFIR irradiation, *Journal of Nuclear Materials*, Vol.179, Part A, 1991, pp.434-437.

[14] Yoon, K. K., Gross, L. B., Wade, C. S. and VanDerSluys, W. A., Evaluation of disk-shaped compact specimen for determining *J-R* curves, *Fracture Mechanics: 26th Volume, ASTM STP 1256*, American Society of Testing and Materials, Philadelphia, 1995, pp.272-283.

[15] Zhang, J.M. and Ardell, A. J., Measurement of the fracture-toughness of CVD-GROWN ZNS using a miniaturized disk-bend test, *Journal of Materials Research*, Vol.6, 1991, pp.1950-1957.

[16] Gilbert, C. J., Cao, J. J., De Jonghe, L. C. and Ritchie, R. O., Crack-growth resistance-curve behavior in silicon carbide: small versus long cracks, *Journal of American Ceramics Society*, Vol.80, 1997, pp.2253-2261.

[17] Betegon, C. and Hancock, J. W., Two parameter characterization of elastic-plastic crack-tip fields. *Journal of Applied Mechanics*, Vol.58, 1991, pp.104-110.

[18] O'Dowd, N. P. and Shih, C. F., Family of crack-tip fields characterized by a triaxiality parameter – I. Structure of fields, *Journal of the Mechanics and Physics of Solids*. Vol.39, 1991, pp.989-1015.

[19] O'Dowd, N. P. and Shih, C. F., Family of crack-tip fields characterized by a triaxiality parameter – II. Fracture applications, *Journal of the Mechanics and Physics of Solids*. Vol.40, 1992, pp.939-963.

[20] Yang, S., Chao, Y. J. and Sutton, M. A., Higher order asymptotic crack tip fields in a power-law hardening material, *Engineering Fracture Mechanics*, Vol.45, 1993a, pp.1-20.

[21] Yang, S., Chao, Y. J. and Sutton, M. A., Complete theoretical analysis for higher order asymptotic terms and the HRR zone at a crack tip for mode I and Mode II loading of a hardening material, *ACTA MECHANICA*, Vol.98, 1993b. pp.79-98.

[22] Chao, Y. J., Yang, S. and Sutton, M. A., On the fracture of solids characterized by one or two parameters: theory and practice, *Journal of the Mechanics and Physics of Solids*, Vol.42, 1994, pp.629-647.

[23] Chao, Y. J. and Zhu, X. K., *J-A_2* Characterization of Crack-Tip Fields: Extent of *J-A_2* Dominance and Size Requirements, *International Journal of Fracture,* Vol.89, 1998, pp.285-307.

[24] Chao, Y.J. and Ji, W., Cleavage fracture quantified by J and A_2, *Constraint Effects in Fracture Theory and Applications: Second Volume, ASTM STP 1244*, American Society of Testing and Materials, Philadelphia, 1995, pp.3-20.

[25] Chao, Y. J. and Lam, P. S., Effects of crack depth, specimen size, and out-of-plane stress on the fracture toughness of reactor vessel steels, *ASME Journal of Pressure and Vessel Technology*, Vol.118, 1996, pp.415-423.

[26] Zhu, X. K. and Chao, Y. J., Characterization of constraint of fully plastic crack-tip fields in non-hardening materials by the three-term solution, to appear in *International Journal of Solids and Structures*, 1999.

[27] Nikishkov, G. P., Bruckner-Foit, A. and Munz, D., Calculation of the second fracture parameter for finite cracked bodies using a three-term elastic-plastic asymptotic expansion, *Engineering Fracture Mechanics*, Vol.52, 1995, pp.685-701.

[28] Yang, S., *Higher order asymptotic crack tip fields in a power-law hardening material*, Ph.D. Dissertation, University of South Carolina, 1993.

[29] Rice, J. R. and Rosengren, G. F., "Plane Strain Deformation near a Crack Tip in a Power Law Hardening Material," *Journal of the Mechanics and Physics of Solids,* Vol.16, pp. 1-12, 1968

[30] Hutchinson, J. W., "Singular Behavior at the End of a Tensile Crack in a Hardening Material," *Journal of the Mechanics and Physics of Solids*, Vol.16, pp. 13-31, 1968.

[31] Hutchinson, J. W., "Plastic Stress and Strain Fields at a Crack Tip," *Journal of the Mechanics and Physics of Solids,* Vol.16, pp. 337-347, 1968.

[32] Chao, Y.J. and Zhang, L., *Tables of plane strain crack tip fields: HRR and higher order terms,* Me-Report, 97-1, Department of Mechanical Engineering, University of South Carolina, 1997.

[33] Ilyushin, A. A., the theory of small elastic-plastic deformations, *Prikadnaia Matematika i Mekhanika, P.M.M.*, Vol.10, 1946, pp.347-356.

[34] Goldman, N. J. and Hutchinson, J. W., Fully plastic crack problems: the center – cracked strip under plane strain, *International Journal of Solids and Structures*, Vol.11, 1975, pp.575-591.

TABLE 1 -- Fracture toughness and constraint quantities for all SENB specimens

Specimen I.D.	a/W	a/b (mm)	J_{IC} (KJ/m^2)	$T_R(\Delta a=1mm)$	Q	A_2
94A	0.29	14.5/35.5	211.8	95.8	-0.36	-0.274
94B	0.26	13.0/37.0	225.6	99.1	-0.43	-0.299
94D	0.19	9.5/40.5	217.2	104.0	-0.60	-0.362
94E	0.39	19.5/30.5	216.0	77.9	-0.24	-0.217
94G	0.55	27.5/22.5	195.2	72.1	-0.15	-0.168
94H	0.55	27.5/22.5	169.2	71.1	-0.10	-0.134
94J	0.13	6.5/43.5	219.3	109.4	-0.70	-0.393
94K	0.14	7.0/43.0	215.1	117.4	-0.70	-0.394
94K	0.14	7.0/43.0	183.0	100.0	-0.67	-0.395
94J	0.13	6.5/43.5	196.5	108.7	-0.68	-0.394
FYB507	0.61	30.5/19.5	189.5	55.0	-0.10	-0.132
95H	0.83	41.5/8.5	162.9	73.7	-0.25	-0.232
95G	0.78	49.0/11.0	145.6	78.7	-0.22	-0.220
95X	0.70	45.0/15.0	172.6	56.1	-0.15	-0.171

Note: the specimen length l = 203mm, l/W = 4, B/W = 0.5; W = 50.mm, B = 25mm. Side groove 20%.

Figure Captions

FIG. 1 – Schematic Regimes for J and J-A2 Controlled Crack Growth.

FIG. 2-- Analysis procedure for constructing the constraint-modified *J-R* curves, equation (24).

(a) Experimental *J-R* curves from various specimens

(b) Determination of the functional relationship $C_0(A_2)$, $C_1(A_2)$, $C_2(A_2)$

FIG. 3 -- Analysis procedure for constructing the constraint-modified *J-R* curves, equation (26).

(a) Determination of the functional relationship between J_{IC} and A_2

(b) Determination of the functional relationship between T_R and A_2

(c) Determination of the functional relationship $C_1(A_2)$, $C_2(A_2)$

FIG. 4 -- Experimental data and fitted curves for SENB specimens. Data points are from Joyce and Link (1997), and the lines are the best-fit curves.

(a) Initiation toughness J_{IC} versus A_2

(b) Tearing toughness T_R versus A_2

FIG. 5 -- Fitted curves for parameters in constraint-modified *J-R* curves with J_{IC} = 194 KJ/m^2 (the dots are calculated from equation (33); the lines are the best-fit curves).

(a) Variation of C_1 versus A_2; (b) Variation of C_2 versus A_2

FIG. 6 -- Fitted curves for parameters in constraint-modified *J-R* curves with

J_{IC} = -119.79 A_2 +161.86 (KJ/m^2)

(the dots are calculated from equation (36); the lines are the best-fit curves).

(a) Variation of C_1 versus A_2; (b) Variation of C_2 versus A_2

FIG. 7 -- Comparisons of predicted *J-R* curves (Equations 35 and 38) and SENB *J-R* curves of Joyce and Link (1997).

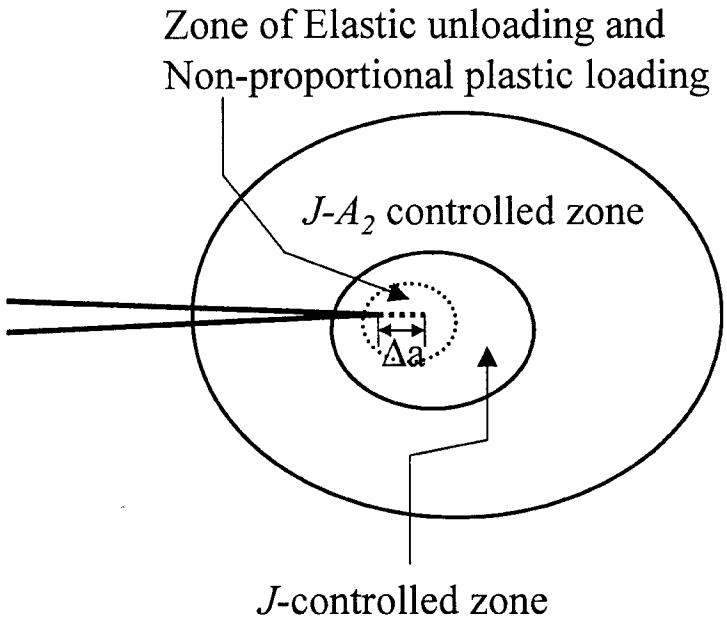

Figure 1 – Schematic Regimes for J and J-A2 Controlled Crack Growth.

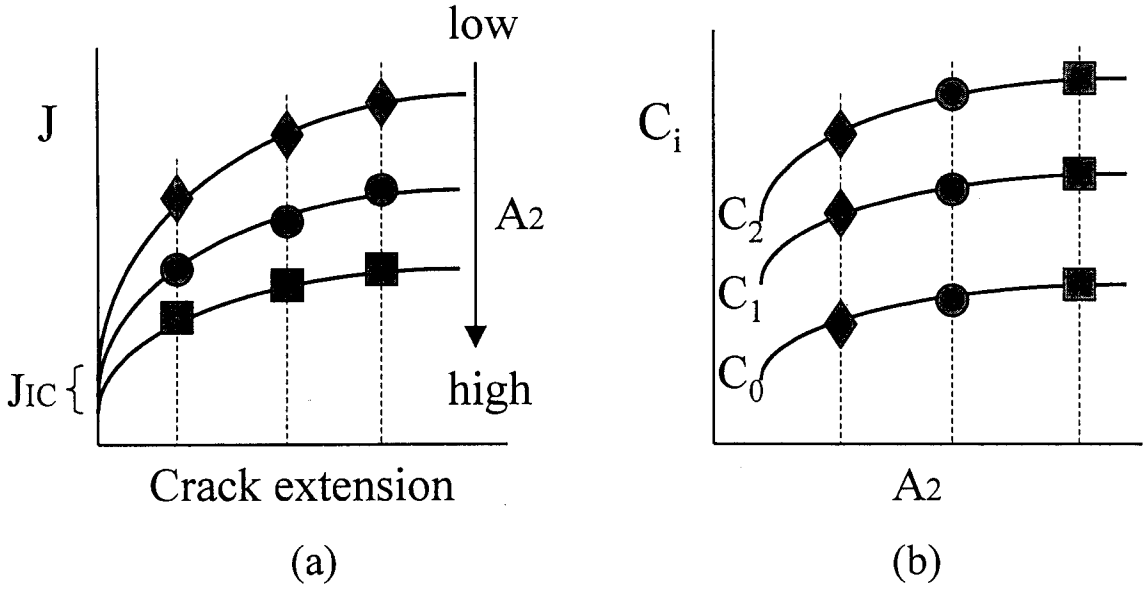

Figure 2-- Analysis procedure for constructing the constraint-modified *J-R* curves, equation (24).
(a) Experimental *J-R* curves from various specimens
(b) Determination of the functional relationship $C_0(A_2)$, $C_1(A_2)$, $C_2(A_2)$

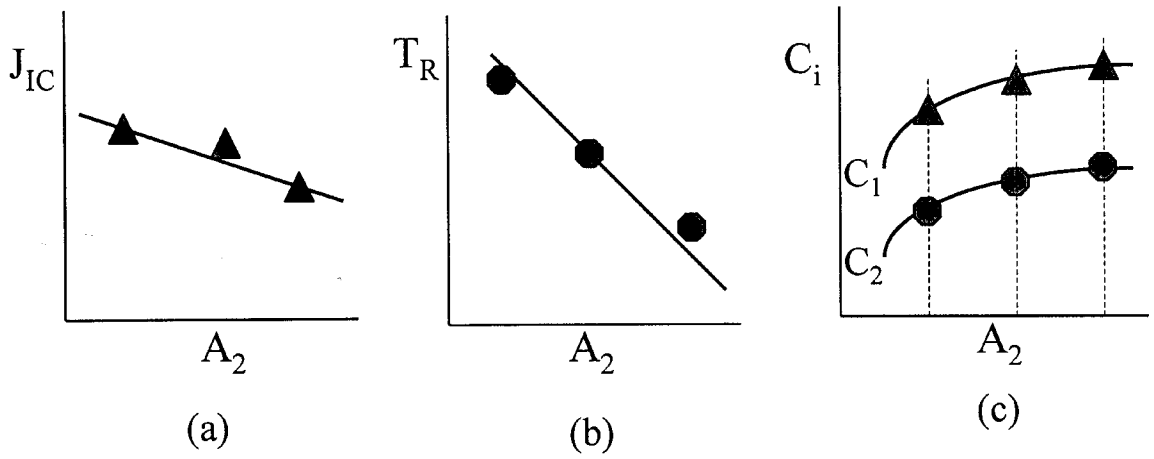

Figure 3 -- Analysis procedure for constructing the constraint modified *J-R* curves, equation (26).
(a) Determination of the functional relationship between J_{IC} and A_2
(b) Determination of the functional relationship between T_R and A_2
(c) Determination of the functional relationship $C_1(A_2)$, $C_2(A_2)$

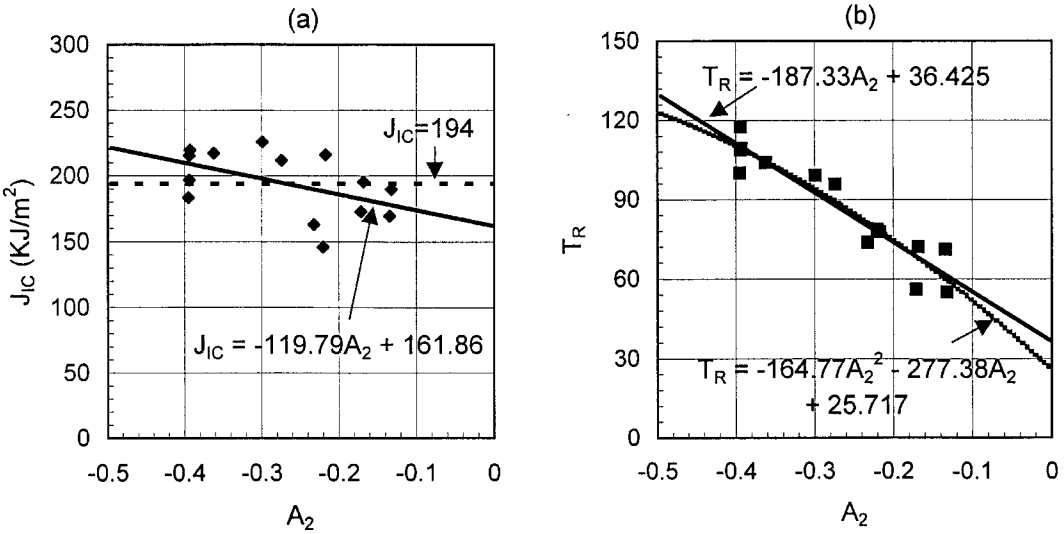

Figure 4 -- Experimental data and fitted curves for SENB specimens. Data points are from Joyce and Link (1997), and the lines are the best-fit curves.
(a) Initiation toughness J_{IC} versus A_2
(b)Tearing toughness T_R versus A_2

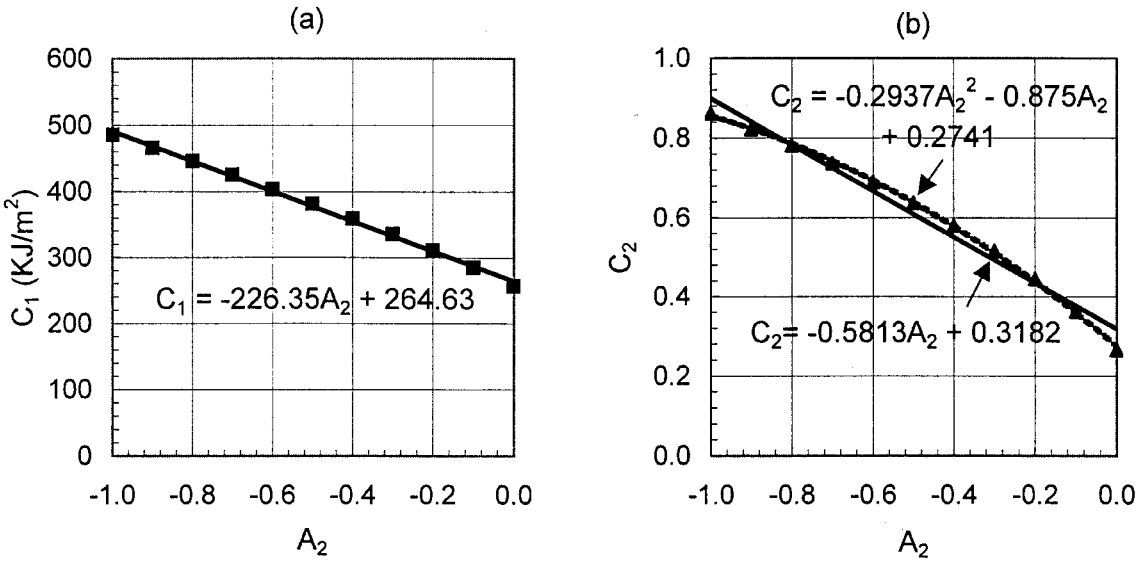

Figure 5 -- Fitted curves for parameters in constraint-modified *J-R* curves with J_{IC} = 194 KJ/m^2
(The dots are calculated from equation (33); the lines are the best-fit curves).
(a) Variation of C_1 versus A_2; (b) Variation of C_2 versus A_2

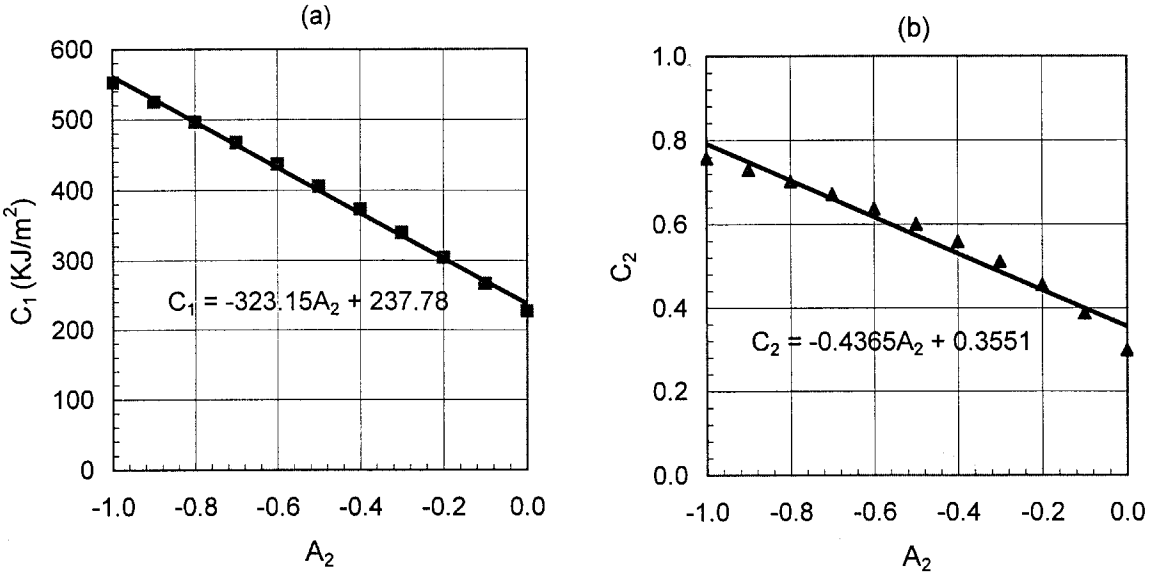

Figure 6 -- Fitted curves for parameters in constraint-modified *J-R* curves with
J_{IC} = -119.79 A_2 +161.86 (KJ/m^2)
(The dots are calculated from equation (36); the lines are the best-fit curves).
(b) Variation of C_1 versus A_2 (b) Variation of C_2 versus A_2

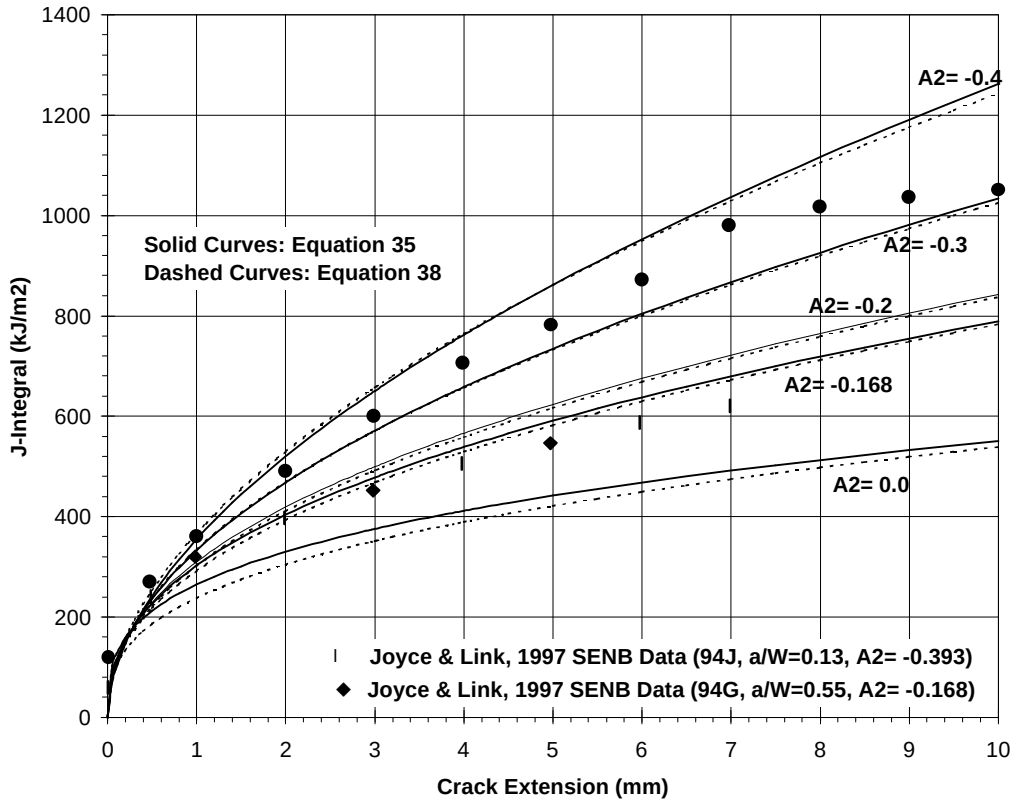

Figure 7 -- Comparisons of predicted *J-R* curves (Equations 35 and 38) and SENB *J-R* curves of Joyce and Link (1997).